Reversed plasma catalysis process design for efficient ammonia decomposition.

*Frea Van Steenweghen[†a], Annabel Verschueren[†a], Igor Fedirchyk[†b], Johan A. Martens[*a], Annemie Bogaerts[b], Lander Hollevoet[a]*

a. Surface Chemistry and Catalysis: Characterization and Application Team (COK-KAT), KU Leuven, Leuven BE-3001 (Belgium).

b. Research group PLASMANT, Department of Chemistry, University of Antwerp, Wilrijk BE-2610 (Belgium).

* E-mail: johan.martens@kuleuven.be

[†]These authors contributed equally.

KEYWORDS

Ammonia decomposition, plasma catalysis, hydrogen production, warm plasma, heterogeneous catalysis, ruthenium catalyst, exergy analysis, heat integration

SYNOPSIS

Reversing the order of plasma and thermocatalytic reactors of an ammonia cracking process reduces the energy need and saves catalyst.

ABSTRACT

An innovative process design for ammonia decomposition through *reversed plasma catalysis* is proposed. *Reversed plasma catalysis* involves a partial thermocatalytic conversion of the ammonia feed prior to a warm plasma conversion process of the residual ammonia. Lab-scale experiments confirm the potential to achieve 98.2% ammonia conversion using a ruthenium-based catalyst in combination with a Gliding Arc Plasmatron (GAP). Process modeling reveals an efficiency gain of using the excess heat available from the warm plasma reactor to support the endothermic thermocatalytic ammonia cracking. In this study, the *reversed plasma catalysis* process was compared to *thermocatalysis* and *plasma catalysis* process designs under identical reactor conditions, revealing similar energy and exergy efficiency for *plasma catalysis* and *reversed plasma catalysis*. The significant advantage of *reversed plasma catalysis* is the major catalyst savings up to 60% compared to *plasma catalysis* and *thermocatalysis*. These catalyst savings also reduce the reactor size, making *reversed plasma catalysis* a promising approach for efficient ammonia decomposition.

INTRODUCTION

Ammonia (NH_3) has emerged as promising hydrogen carrier due to its high volumetric hydrogen atom content, ease of liquefaction, and existing infrastructure [1–4]. The key remaining challenge is the development of technology for large-scale ammonia decomposition. Substantial research efforts are being directed toward developing affordable, energy-efficient, and flexible ammonia decomposition processes [1,4,5].

The most widely explored option is thermocatalytic cracking, but it is limited by the thermodynamic equilibrium of maximum ammonia conversion levels [6]. The NH_3 decomposition reaction is thermodynamically favored at elevated temperatures (> 300°C) and low pressures (1 bar) [7]. At 350°C, the theoretical maximum conversion is limited to 99%. In theory, gaining additional conversion up to, e.g., 99.9% necessitates heating to 530°C. In practice, achieving such high NH_3 conversion requires temperatures of 600-800°C [8]. Heating the gas feed and catalyst bed to such high temperatures requires energy and, therefore, reduces energy efficiency. Operation at high temperatures also limits the catalyst lifetime. Moreover, elevated temperatures are typically generated by combusting fuel, which may be natural gas or the hydrogen (H_2) product itself, or the NH_3 feed [8,9]. The first option entails CO_2 emission, causing the process to lose its green label, while the second and third option lower the hydrogen yield. One way to reduce the required temperature while maintaining high NH_3 conversions is to increase the residence time, which can be achieved by enlarging the reactor and increasing the amount of catalyst [10]. However, this significantly impacts the cost.

Plasma technology is a promising alternative to overcome thermodynamic limitations of endothermic cracking reactions. Plasma is an ionized gas with free electrons, ions, radicals, vibrationally and electronically excited molecules, and photons [11,12]. The energetic electrons activate molecules of the gas which itself does not have to be heated [12]. Additionally, plasma reactors are powered by electricity and can be quickly switched on/off, enabling the utilization of renewable intermittent electricity sources [11,13].

Plasmas are classified into three main types: *cold*, which has high-energy electrons but keeps gas molecules unheated; *thermal*, in which the electrons and gas molecules reach similar high temperature (~10,000°C); and *warm*, with similar electron temperatures but with gas

temperatures below ~5,000°C [14]. Due to the low gas temperature in cold plasma, non-equilibrium conditions caused by molecular transformations persist best in the reaction products [12]. In the case of ammonia decomposition, state-of-the-art *cold* plasma processes do not meet the high conversion and low energy consumption requirements [15]. The reason is that the electrons mainly give rise to electronic excitation and ionization, which requires more energy than is strictly needed, and this excess energy is wasted. Vibrational excitation is more important in warm plasma. In warm plasma, the product composition may reflect the thermodynamic equilibria at very high temperatures, overcoming the thermodynamic equilibrium limitations of the NH_3 decomposition reaction at lower temperatures [16]. Thus, the NH_3 decomposition process in warm plasma is free from the influence of reverse reaction, which is not thermodynamically favored in these conditions. Nevertheless, warm plasma struggles to reach high NH_3 conversions despite its more favorable energy consumption [14].

The combined use of plasma and catalyst in so-called *plasma catalysis* has been proposed to improve the performance of chemical conversion processes. Plasma enables additional reaction pathways, which may be unavailable on solid catalysts [17]. Positioning a catalyst inside plasma is possible in *cold* plasma reactors, such as those with dielectric barrier discharge (DBD), which are the most studied subset of reactors for *plasma-catalytic* NH_3 cracking (**Table 1**). For instance, Wang *et al.* (2024) reached about 100% conversion, but at the expense of a high energy cost of 888 $kJ.mol_{NH3}^{-1}$ using a DBD featuring an in-plasma Mo_2N catalyst [18]. The research into *plasma-catalytic* conversion in warm plasmas has been limited to a few works using gliding arc (GA) reactors in post-plasma configuration. In one case, a *warm* plasma reactor of the non-thermal arc plasma type (NTAP) having a post-plasma NiO/Al_2O_3 catalyst has been reported achieving a record low energy cost of 157 $kJ.mol_{NH3}^{-1}$, but the NH_3 conversion was limited to ca. 20% [19].

Plasma catalysis, such as DBD with an in-plasma catalyst, can achieve high conversions but has very low energy efficiency [20,21]. Moreover, the physical combination of plasma and catalyst may present challenges for catalyst stability, especially in conditions provided by warm plasma [22,23].

Table 1: Overview of experimental atmospheric-pressure *plasma-catalytic* NH_3 cracking from literature. Energy cost ($kJ.mol_{NH3}^{-1}$) does not include compression of product gas from 0.1 MPa to 5 MPa.

Plasma	Catalyst	Design	NH_3 feed concentration (%)	T_o (°C)	NH_3 Conv. (%)	Energy cost ($kJ.mol_{NH3}^{-1}$)	Ref.
DBD	Fe_2N	In-plasma	100	410	100	841	[24]
DBD	Co/SiO_2	In-plasma	100	450	99.2	755	[25]
DBD	$Fe\text{-}Ni/SiO_2$	In-plasma	100	500	100	540	[26]
DBD	Co/SiO_2	In-plasma	100	380	98	343	[27]
DBD	Ru/Al_2O_3	In-plasma	0.5	RT	86	157,000	[28]
DBD	$MgAl_2O_4$	In-plasma	100	RT	15.1	2,494	[29]
DBD	Ru/La_2O_3	In-plasma	100	380	99.9	404	[30]
DBD	Ru/La_2O_3	In-plasma	100	RT	20	2,017	[30]
DBD	Mo_2N	In-plasma	100	490	92	1,462	[31]
DBD	Mo_2N	In-plasma	100	RT	100	888	[32]
DBD	Ni/Al_2O_3	In-plasma	15	435	99.6	3,601	[18]
NTAP	NiO/Al_2O_3	Post-plasma	100	RT	20	157	[19]
GA	$Ba\text{-}Co/CeO_2$	Post-plasma	50	RT	70	384	[33]

We propose an alternative process design for ammonia decomposition, namely *reversed plasma catalysis*, having a thermocatalyst positioned in front of the plasma reactor instead of inside or

after (**Figure 1**) [34]. A complex sort of *reversed plasma catalysis* having a thermocatalyst (Ni/Al_2O_3) in front of a plasma membrane reactor achieving decomposition combined with hydrogen separation through a membrane has been proposed in literature [35]. High NH_3 conversion levels of up to 99.9% were reached, but the energy consumption was high, viz. 696 $kJ.mol_{NH3}^{-1}$ [36]. Evidence for clear advantages of reversing the order of the processes has not yet been provided.

The concept of *reversed plasma catalysis* was evaluated through a combination of experiments and computational simulation. *Reversed plasma catalysis* was compared *to thermocatalysis* and *plasma catalysis* regarding energy and exergy use ($kJ.mol_{NH3}^{-1}$), and catalyst use ($g_{cat}.h.mol_{NH3}^{-1}$). The latter parameter also reflects the required thermocatalytic reactor size.

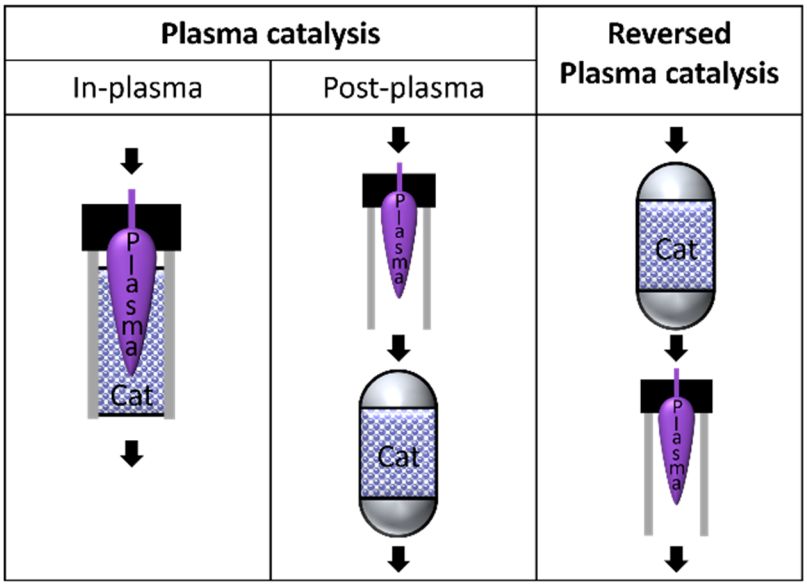

Figure 1: *Plasma catalysis* (in-plasma and post-plasma) and *reversed plasma catalysis* process designs.

RESULTS AND DISCUSSION

Partial NH_3 cracking can be conducted efficiently on a thermocatalyst without requiring temperatures exceeding 500°C, avoiding expensive reactor construction materials [7,37]. Reaching the NH_3 conversion limit dictated by the thermodynamic equilibrium between ammonia and its decomposition products is very demanding for a thermocatalytic reactor. Conversely, plasma is energy-intensive for converting NH_3, but it is well-suited for achieving the conversion of the residual unconverted NH_3 left over after a thermocatalytic decomposition. Plasma operates on electric power, which is partially converted into chemical energy in the endothermic NH_3 cracking reaction and partially converted into heat, especially in thermal and warm plasma [38]. This excess heat can serve as a heat source for the endothermic thermocatalytic process. Moreover, plasma reactors have a simple design, and don't need expensive materials [39]. The power supply constitutes the primary contributor to the capital cost of the plasma reactor, which is expected to decrease with technological advancements and large-scale adoption of plasma technology, ultimately resulting in a lower overall CAPEX.

A particularly effective catalyst described in literature was selected, viz. potassium-promoted ruthenium on alumina [7,40]. The catalyst, denoted as $10K/5Ru/Al_2O_3$, was synthesized using incipient wetness impregnation of subsequently Ru and K precursors onto alumina with nominal weight ratios of 10/5/100. The catalytic performance was evaluated in a continuous flow fixed bed microreactor using pure NH_3 flow. Experimental details can be found in the supplementary information (SI, section 1).

The most efficient warm plasma reactor type was found to be the Gliding Arc Plasmatron (GAP) [14], which was also proven effective for other gas conversion applications [41–43]. This plasma

reactor was fed with a gas mixture simulating the outlet of the thermocatalytic reactor. Experimental details can be found in the SI (section 2).

The thermocatalytic reactor reached an NH_3 conversion of 92.3% at 410°C at a WHSV of 4.4 h^{-1} (GHSV of 5,800 $mL_{NH3}.g_{cat}^{-1}.h^{-1}$). The reaction product has a gas composition of 4 vol% NH_3, 72 vol% H_2, and 24 vol% N_2. Using such mixture as feed, the GAP plasma reactor decomposed 77.2% of the NH_3 contained in this gas mixture at a reaction rate of 0.06 $mol_{NH3}.h^{-1}$ with an energy consumption of 1,600 kJ per mol of cracked NH_3 by plasma. Based on literature data [44–46], specifications of existing commercial plasma devices (e.g., Hypertherm HPR400XD, Oerlikon-Metco FlexiArc™ 300), and experimental results obtained with suboptimally matched power supplies [14], it can be reasonably assumed that, with proper matching to the plasma setup, the power supply efficiency can reach at least 90%. Using this efficiency value as a baseline, the actual energy consumption amounts to 1,750 kJ per mol of cracked NH_3 by plasma. This energy requirement pertains to the two reactors in the *reversed plasma catalysis* process, as the plasma reactor delivers the heat for the thermocatalytic reactor. Consequently, the overall energy cost of cracking the ammonia feed is 105 kJ per mol NH_3 converted through *reversed plasma catalysis*.

Figure 2 represents the process scheme of the *reversed plasma catalysis* process with a thermocatalytic reactor (1) followed by a GAP plasma reactor (2). A heat exchanger (3) is added to recover the heat generated in the plasma reactor and use it to heat the thermocatalytic reactor. A compressor (4) is added to compress the produced gas to 5 MPa.

The *reversed plasma catalysis* process was simulated using the Aspen Plus V14 software. The input data can be found in SI (section 3, Table S1). The feed is liquid pure NH_3 at -33°C and atmospheric pressure [1]. The cold NH_3 feed is evaporated and heated to 410°C via heat exchangers with heat coming from the compressor and the hot product gas. Well-insulated heat exchangers

were assumed with a significant temperature difference between the hot inlet and cold outlet. The hot feed is directed into the thermocatalytic reactor, decomposing 92.3% of the pure NH_3 feed. The outlet gas mixture contains 4 vol% NH_3 and is fed into the GAP plasma reactor, which converts 77.2% of this remaining NH_3. The plasma reactor is simulated as a combination of a heater and a reactor making no by-products. The hot product gas of the plasma reactor has an outlet temperature of about 2000°C, which agrees well with literature-based experiments with the same plasma reactor [47]. The hot gas serves as a heat source for maintaining the catalytic reactor at its operating temperature of 410°C and preheating the NH_3 feed. The overall NH_3 conversion reaches 98.2%, of which 92.3% is achieved by thermocatalysis and 5.9% by warm plasma. The final gas composition at the outlet of the *reversed plasma catalysis* process corresponds to 0.9 vol% NH_3, 74.3 vol% H_2, and 24.8 vol% N_2. The remaining 0.9 vol% NH_3 in the gas product could be purified downstream using separation techniques, such as adsorption [7,48,49]. However, approaching full conversion in a single pass process is crucial to avoid significant energy penalties and increased complexity associated with the additional separation steps and the recirculation of large quantities of ammonia. A 4-stage compressor located downstream compresses the product gas to 5 MPa, the desired gas pressure in hydrogen pipelines [50]. Four stages are needed due to the maximal allowable discharge temperature of around 150°C in reciprocating compressors [51]. The additional heat created by the compressor is used to evaporate the liquid NH_3 feed.

The energy consumed by the different unit operations: evaporation and heating of the feed, the heat requirement for the endothermic cracking reaction in the catalytic reactor, and work for operating the plasma reactor as well as the compressor is presented in **Figure 3**. The excess heat generated by plasma and compressor can be recovered as heat required for NH_3 evaporation,

preheating and catalytic cracking. Therefore, the net energy consumption (136 $kJ.mol_{NH3}^{-1}$) is entirely determined by the plasma process (105 $kJ.mol_{NH3}^{-1}$) and compression (31 $kJ.mol_{NH3}^{-1}$).

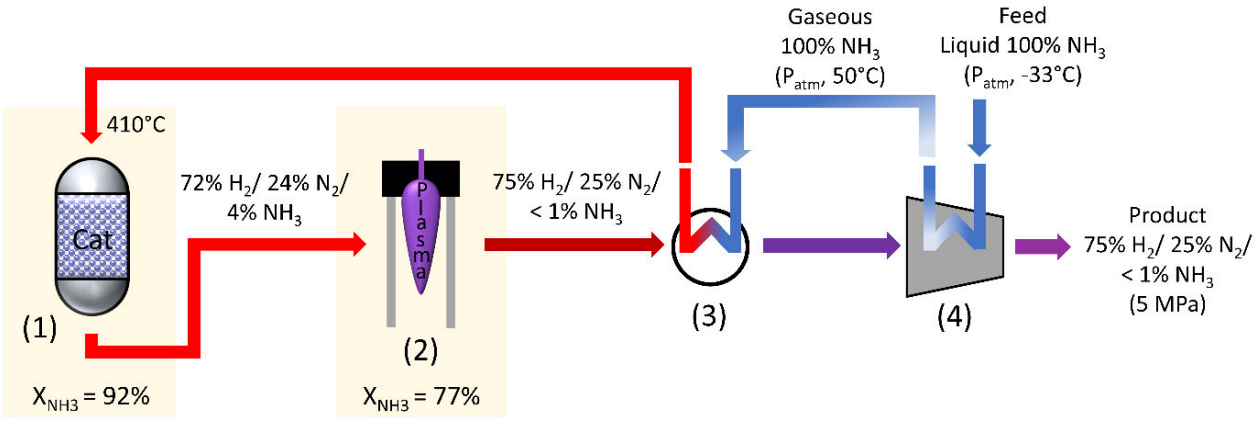

Figure 2: Scheme of *reversed plasma catalysis* process, comprising a thermocatalytic reactor with 10K/5Ru/Al_2O_3 catalyst (1), a GAP plasma reactor (2), a heat exchanger (3) and a compressor (4). Conversions are obtained from experimental data. Heat integration is indicated by heat exchangers between compressor and liquid feed, and hot plasma outlet stream and gaseous feed.

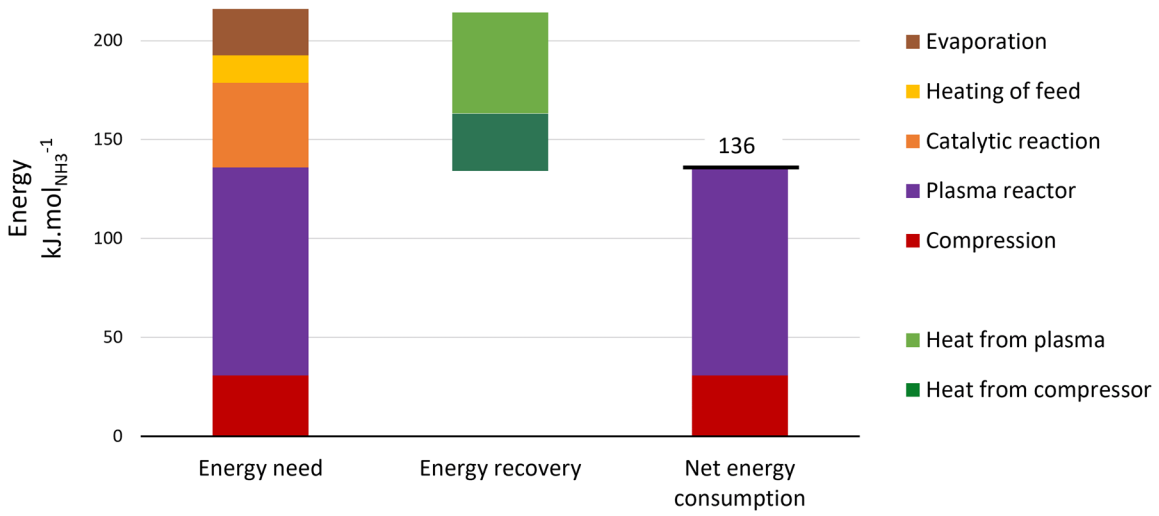

Figure 3: Energy requirements of *reversed plasma catalysis* process with energy recovery.

To demonstrate the potential of the *reversed plasma catalysis* process, it was experimentally compared to both the *thermocatalysis* and *plasma catalysis* (post-plasma) process designs. The processes were operated under identical conditions: at the same current and gas flow rate for the GAP plasma reactor and the same temperature for the catalytic reactor. In all cases, the NH_3 conversion reached 98.2%. The plasma process alone was disregarded as it was not able to reach the 98.2% conversion target as standalone technology. More specifically, the GAP plasma reactor, operating under the same conditions, reaches only 24% conversion of pure NH_3 with an energy consumption of 231 kJ per mol NH_3 converted in the plasma reactor.

The thermocatalytic process achieves the target 98.2% NH_3 conversion at 410°C at a WHSV of 1.6 h^{-1}, corresponding to a catalyst contact time of 10.6 $g_{cat}.h.mol_{NH3}^{-1}$. In this process design, no smart heat integration is possible, necessitating external heating for both the feed and catalytic reactor. In the *plasma catalysis* process, the GAP reactor decomposes 38% of the NH_3 feed with an energy consumption of 230 kJ per mol NH_3 converted by plasma operated at 644 W. In order to obtain the 98.2% overall conversion, the catalyst has to decompose 97.1% of the remaining NH_3, which, at 410 °C, could be reached at a WHSV of 1.9 h^{-1}, corresponding to a catalyst contact time of 8.8 $g_{cat}.h.mol_{NH3}^{-1}$.

The experimental results were further analyzed through process simulations in Aspen Plus to determine the net energy consumption, incorporating smart heat integration between the plasma and catalytic reactors, as well as between the compressor and feed. The process schemes made by Aspen for the three process designs can be found in SI (section 3). However, a more significant parameter for evaluating these processes is the net exergy consumption, which accounts for the useful excess heat generated [52]. Net exergy consumption is determined by subtracting the useful

exergy output from total exergy input. The total exergy input is the electricity powering the plasma reactor and compressor, along with the chemical exergy of the NH_3 feed. The useful exergy output consists of the chemical exergy of the product and the exergy of the excess heat, which increases with its temperature [53,54]. Detailed calculations are provided in SI (section 4). The net energy consumption, net exergy consumption and catalyst need for the three processes are summarized in **Table 2**.

Table 2: Comparison of process performance characteristics to obtain a 98.2% overall NH_3 conversion with 100% liquid NH_3 feed and 5 MPa product pressure for *thermocatalysis* (10K/5Ru/Al_2O_3, 410°C), *plasma catalysis* (GAP, 10 nL.min^{-1} NH_3 flow rate, 644 W – 10K/5Ru/Al_2O_3, 410°C) and *reversed plasma catalysis* (10K/5Ru/Al_2O_3, 410°C - GAP, 20 nL.min^{-1} total flow rate with 4 vol% NH_3, 723W)

Process design	***Thermocatalysis***	***Plasma catalysis* (post-plasma)**	***Reversed plasma catalysis***
Net energy consumption ($kJ.mol_{NH3}^{-1}$)	78.2	128	136
Net exergy consumption ($kJ.mol_{NH3}^{-1}$)	46.3	60.4	60.5
Catalyst need ($g_{cat}.h.mol_{NH3}^{-1}$)	10.6	8.8	3.9

In terms of net energy consumption, the thermocatalysis process remains the most efficient. *Plasma catalysis* shows a slightly lower energy consumption than the reversed process, due to the higher efficiency of the plasma reactor when operating with a pure NH_3 feed. In addition, both *plasma catalysis* and *reversed plasma catalysis* processes from this study outperform plasma-

based processes reported in the literature (**Table 1**), which predominantly use cold plasma. The superior performance can be attributed to the benefits of using a warm plasma, *i.e.,* its higher energy efficiency and effective utilization of excess heat as a source for catalytic cracking. Moreover, none of the processes reported in literature account for the energy cost of compressing the hydrogen product. The similar net exergy consumption for the *plasma catalysis* and *reversed plasma catalysis* concepts reflects the high-quality heat generated in the *reversed plasma catalysis* process. To further optimize energy and exergy consumption, plasma energy consumption should ideally approach the theoretical minimum of 55 $kJ.mol_{NH3}^{-1}$.

The most salient feature of *reversed plasma catalysis* is its drastically lower catalyst requirement, which is two times lower than in *plasma catalysis* and almost three times lower than in *thermocatalysis*. Positioning the catalyst upstream of the plasma reactor not only reduces the catalyst cost but also the size of the thermocatalytic reactor, significantly lowering installation costs. While *thermocatalysis* exhibits lower energy consumption, the *reversed plasma catalysis* process stands out due to its significantly reduced catalyst demand, enabling a much smaller catalytic reactor size. Future improvements in energy efficiency of the plasma reactor can reduce the amount of excess heat generated, and therefore lower the energy cost while maintaining the same advantage in smaller reactor size.

CONCLUSIONS

This study highlights the potential of *reversed plasma catalysis* as an alternative ammonia decomposition process design. The innovative *reversed plasma catalysis* process allows the use of the excess heat created by warm plasma in the catalytic process, resulting in high conversions at moderate catalyst temperature (410°C). An overall conversion of 98.2% was achieved, with 92%

accomplished through ruthenium-based thermocatalysis and 6% through warm plasma. As a future perspective, replacing ruthenium with a non-precious metal is a viable strategy because of the low temperature (410°C) and the moderate conversion rate requirement (92%) in the thermocatalytic reactor (**Figure 2**).

A comparative study of *plasma catalysis* and *reversed plasma catalysis* revealed similar net energy and exergy consumption, which are both substantially lower than previously reported in the literature (**Table 1**). However, compared to *thermocatalysis*, the *reversed plasma catalysis* process is not yet as energy efficient. Improving the energy efficiency of the plasma reactor will be crucial for enhancing the overall energy performance. Notably, the *reversed plasma catalysis* process requires only half of the catalyst mass needed in *plasma catalysis* and almost one-third of that in *thermocatalysis* (**Table 2**). This results in substantial catalyst savings and downsizing of the reactor. This advantage positions the *reversed plasma catalysis* process as a competitive alternative for ammonia decomposition.

ASSOCIATED CONTENT

Supporting Information.

The supplementary Information file (PDF) is available free of charge and contains following sections:

Section 1 & 2: Detailed experimental procedures for thermocatalytic cracking and plasma cracking, including lab setup, operating conditions, and catalyst description

Section 3: Aspen Plus input data used for process modeling and simulation of the reversed plasma catalysis process, including component specifications and process parameters. And Aspen plus process schemes for the three compared processes

Section 4: Exergy analysis of the three compared processes, including equations and results.

AUTHOR INFORMATION

Corresponding Author

Prof. Johan A. Martens: Johan.martens@kuleuven.be

Author Contributions

F.V.S. †: investigation, data curation, visualization, funding acquisition, writing – original draft. A.V. †: investigation, data curation. I.F. †: investigation, data curation, funding acquisition, writing – original draft. J.A.M.: supervision, project administration, funding acquisition, writing – review & editing. A.B.: supervision, project administration, funding acquisition, writing – review & editing. L.H.: formal analysis, conceptualization, validation, funding acquisition, writing – review & editing. All authors have given approval to the final version of the manuscript. †These authors contributed equally.

Conflicts of interest

There are no conflicts to declare.

ACKNOWLEDGMENTS

This work was supported by the HyPACT project funded by the Belgian Energy Transition Fund. J.A.M. and A.B. gratefully acknowledge the Flemish Government for long-term

structural funding (Methusalem). J.A.M. acknowledges KU Leuven for an internal grant from the Industrial Research Fund (project No. C3/20/067). F.V.S. acknowledges Research Foundation Flanders (FWO) for an FWO-SB fellowship (No. 1S58723N). L.H. also acknowledges Flanders Innovation & Entrepreneurship for an innovation mandate (No. HBC.2023.0674). I.F. acknowledges the MSCA4Ukraine project 1233629 funded by the European Union.

ABBREVIATIONS

NH_3, ammonia; H_2, hydrogen; N_2, nitrogen.

REFERENCES

(1) International Renewable Energy Agency (IRENA); Ammonia Energy Association (AEA). *Innovation Outlook: Renewable Ammonia*; Abu Dhabi, Brooklyn, 2022; Vol. 144.

(2) Hasan, M. H.; Mahlia, T. M. I.; Mofijur, M.; Rizwanul Fattah, I. M.; Handayani, F.; Ong, H. C.; Silitonga, A. S. A Comprehensive Review on the Recent Development of Ammonia as a Renewable Energy Carrier. *Energies (Basel)* **2021**, *14* (13), 3732. https://doi.org/10.3390/en14133732.

(3) Cha, J.; Jo, Y. S.; Jeong, H.; Han, J.; Nam, S. W.; Song, K. H.; Yoon, C. W. Ammonia as an Efficient CO_X-Free Hydrogen Carrier: Fundamentals and Feasibility Analyses for Fuel Cell Applications. *Appl Energy* **2018**, *224*, 194–204. https://doi.org/10.1016/j.apenergy.2018.04.100.

(4) Spatolisano, E.; Pellegrini, L. A.; De Angelis, A. R.; Cattaneo, S.; Roccaro, E. Ammonia as a Carbon-Free Energy Carrier: NH_3 Cracking to H_2. *Ind Eng Chem Res* **2023**, *62* (28), 10813–10827. https://doi.org/10.1021/acs.iecr.3c01419.

(5) Weichenhain, U. *Hydrogen Transportation*. https://www.rolandberger.com/en/Insights/Publications/Transporting-the-fuel-of-the-future.html (accessed 2024-05-22).

(6) Li, N.; Zhang, C.; Li, D.; Jiang, W.; Zhou, F. Review of Reactor Systems for Hydrogen Production via Ammonia Decomposition. *Chemical Engineering Journal* **2024**, 153125. https://doi.org/10.1016/j.cej.2024.153125.

(7) Lucentini, I.; Garcia, X.; Vendrell, X.; Llorca, J. Review of the Decomposition of Ammonia to Generate Hydrogen. *Ind Eng Chem Res* **2021**, *60* (51), 18560–18611. https://doi.org/10.1021/acs.iecr.1c00843.

(8) Yousefi Rizi, H.; Shin, D. Green Hydrogen Production Technologies from Ammonia Cracking. *Energies (Basel)* **2022**, *15* (21), 8246. https://doi.org/10.3390/en15218246.

(9) Kang, Z.; Liu, B.; Huang, J.; Fan, H.; Wang, K. A Hydrogen Production System Based on Ammonia Combustion Heat: Graded Decomposition and Parameter Analysis. *E3S Web of Conferences* **2024**, *520*, 03010. https://doi.org/10.1051/e3sconf/202452003010.

(10) Chein, R. Y.; Chen, Y. C.; Chang, C. S.; Chung, J. N. Numerical Modeling of Hydrogen Production from Ammonia Decomposition for Fuel Cell Applications. *Int J Hydrogen Energy* **2010**, *35* (2), 589–597. https://doi.org/10.1016/j.ijhydene.2009.10.098.

(11) Bogaerts, A.; Centi, G.; Hessel, V.; Rebrov, E. Challenges in Unconventional Catalysis. *Catal Today* **2023**, *420*, 114180. https://doi.org/10.1016/j.cattod.2023.114180.

(12) Bogaerts, A.; Neyts, E. C. Plasma Technology: An Emerging Technology for Energy Storage. *ACS Energy Lett* **2018**, *3* (4), 1013–1027. https://doi.org/10.1021/acsenergylett.8b00184.

(13) Bogaerts, A.; Centi, G. Plasma Technology for CO2 Conversion: A Personal Perspective on Prospects and Gaps. *Front Energy Res* **2020**, *8* (111). https://doi.org/10.3389/fenrg.2020.00111.

(14) Fedirchyk, I.; Tsonev, I.; Quiroz Marnef, R.; Bogaerts, A. Plasma-Assisted NH3 Cracking in Warm Plasma Reactors for Green H2 Production. *Chemical Engineering Journal* **2024**, *499*, 155946. https://doi.org/10.1016/j.cej.2024.155946.

(15) Gorbanev, Y.; Fedirchyk, I.; Bogaerts, A. Plasma Catalysis in Ammonia Production and Decomposition: Use It, or Lose It? *Curr Opin Green Sustain Chem* **2024**, *47*, 100916. https://doi.org/10.1016/j.cogsc.2024.100916.

(16) Gutsol, A.; Rabinovich, A.; Fridman, A. Combustion-Assisted Plasma in Fuel Conversion. *J Phys D Appl Phys* **2011**, *44* (27), 274001. https://doi.org/10.1088/0022-3727/44/27/274001.

(17) Bogaerts, A.; Tu, X.; Whitehead, J. C.; Centi, G.; Lefferts, L.; Guaitella, O.; Azzolina-Jury, F.; Kim, H.-H.; Murphy, A. B.; Schneider, W. F.; Nozaki, T.; Hicks, J. C.; Rousseau, A.; Thevenet, F.; Khacef, A.; Carreon, M. The 2020 Plasma Catalysis Roadmap. *J Phys D Appl Phys* **2020**, *53* (44), 443001. https://doi.org/10.1088/1361-6463/ab9048.

(18) Zhou, W.; Zhang, W.; Shan, Y.; Liu, B.; Li, K.; Ren, J.; Li, Y.; Zhang, X.; Wang, Z. Carbon-Free Hydrogen Production via Plasma-Catalytic Ammonia Decomposition over Transition Metal-Based Catalysts: In Situ Probing by DRIFTS and SVUV-PIMS. *Chemical Engineering Journal* **2024**, *492*, 152101. https://doi.org/10.1016/j.cej.2024.152101.

(19) Lin, Q. F.; Jiang, Y. M.; Liu, C. Z.; Chen, L. W.; Zhang, W. J.; Ding, J.; Li, J. G. Instantaneous Hydrogen Production from Ammonia by Non-Thermal Arc Plasma

Combining with Catalyst. *Energy Reports* **2021**, *7*, 4064–4070. https://doi.org/10.1016/j.egyr.2021.06.087.

(20) Meng, S.; Li, S.; Sun, S.; Bogaerts, A.; Liu, Y.; Yi, Y. NH_3 Decomposition for H_2 Production by Thermal and Plasma Catalysis Using Bimetallic Catalysts. *Chem Eng Sci* **2024**, *283*, 119449. https://doi.org/10.1016/j.ces.2023.119449.

(21) Yi, Y.; Wang, L.; Guo, H. Plasma-Catalytic Decomposition of Ammonia for Hydrogen Energy. In *Plasma Catalysis: Fundamentals and Applications*; Tu, X., Whitehead, J. C., Nozaki, T., Eds.; Springer International Publishing: Cham, 2019; pp 181–230.

(22) Zhang, S.; Oehrlein, G. S. From Thermal Catalysis to Plasma Catalysis: A Review of Surface Processes and Their Characterizations. *J Phys D Appl Phys* **2021**, *54* (21), 213001. https://doi.org/10.1088/1361-6463/abe572.

(23) Loenders, B.; Michiels, R.; Bogaerts, A. Is a Catalyst Always Beneficial in Plasma Catalysis? Insights from the Many Physical and Chemical Interactions. *Journal of Energy Chemistry* **2023**, *85*, 501–533. https://doi.org/10.1016/j.jechem.2023.06.016.

(24) Wang, L.; Zhao, Y.; Liu, C.; Gong, W.; Guo, H. Plasma Driven Ammonia Decomposition on a Fe-Catalyst: Eliminating Surface Nitrogen Poisoning. *Chemical Communications* **2013**, *49* (36), 3787. https://doi.org/10.1039/c3cc41301b.

(25) Wang, L.; Yi, Y.; Zhao, Y.; Zhang, R.; Zhang, J.; Guo, H. NH_3 Decomposition for H_2 Generation: Effects of Cheap Metals and Supports on Plasma–Catalyst Synergy. *ACS Catal* **2015**, *5* (7), 4167–4174. https://doi.org/10.1021/acscatal.5b00728.

(26) Yi, Y.; Wang, L.; Guo, Y.; Sun, S.; Guo, H. Plasma-assisted Ammonia Decomposition over Fe–Ni Alloy Catalysts for CO_x-Free Hydrogen. *AIChE Journal* **2018**, *65* (2), 691–701. https://doi.org/10.1002/aic.16479.

(27) Wang, L.; Yi, Y.; Guo, H.; Du, X.; Zhu, B.; Zhu, Y. Highly Dispersed Co Nanoparticles Prepared by an Improved Method for Plasma-Driven NH3 Decomposition to Produce H2. *Catalysts* **2019**, *9* (2), 107. https://doi.org/10.3390/catal9020107.

(28) El-Shafie, M.; Kambara, S.; Hayakawa, Y. Plasma-Enhanced Catalytic Ammonia Decomposition over Ruthenium (Ru/Al2O3) and Soda Glass (SiO2) Materials. *Journal of the Energy Institute* **2021**, *99*, 145–153. https://doi.org/10.1016/j.joei.2021.09.001.

(29) Andersen, J. A.; Christensen, J. M.; Østberg, M.; Bogaerts, A.; Jensen, A. D. Plasma-Catalytic Ammonia Decomposition Using a Packed-Bed Dielectric Barrier Discharge Reactor. *Int J Hydrogen Energy* **2022**, *47* (75), 32081–32091. https://doi.org/10.1016/j.ijhydene.2022.07.102.

(30) Wang, Z.; He, G.; Zhang, H.; Liao, C.; Yang, C.; Zhao, F.; Lei, G.; Zheng, G.; Mao, X.; Zhang, K. Plasma-Promoted Ammonia Decomposition over Supported Ruthenium Catalysts for COx -Free H2 Production. *ChemSusChem* **2023**, *16* (24), e202202370. https://doi.org/10.1002/cssc.202202370.

(31) Yu, X.; Hu, K.; Zhang, H.; He, G.; Xia, Y.; Deng, M.; Shi, Y.; Yang, C.; Mao, X.; Wang, Z. Plasma-Catalytic Ammonia Decomposition for Carbon-Free Hydrogen Production Using Low Pressure-Synthesized Mo_2N Catalyst. *Plasma Chemistry and Plasma Processing* **2023**, *43* (1), 183–197. https://doi.org/10.1007/s11090-022-10282-y.

(32) Wang, Z.; Zhang, H.; Ye, Z.; He, G.; Liao, C.; Deng, J.; Lei, G.; Zheng, G.; Zhang, K.; Gou, F.; Mao, X. H2 Production from Ammonia Decomposition with Mo2N Catalyst Driven by Dielectric Barrier Discharge Plasma. *Int J Hydrogen Energy* **2024**, *49*, 1375–1385. https://doi.org/10.1016/j.ijhydene.2023.06.173.

(33) Ronduda, H.; Młotek, M.; Góral, W.; Zybert, M.; Ostrowski, A.; Sobczak, K.; Krawczyk, K.; Raróg-Pilecka, W. Cobalt Catalysts for CO -Free Hydrogen Production: Effect of Catalyst Type on Ammonia Decomposition in Gliding Discharge Plasma Reactor. *Journal of CO2 Utilization* **2024**, *82*, 102755. https://doi.org/10.1016/j.jcou.2024.102755.

(34) Drake, G. W. F.; Babb, J.; Bandrauk, A. D.; Joachain, C. J. *Plasma Catalysis: Fundamentals and Applications*, 1st ed.; Tu, X., Nozaki, T., Whitehead, J. C., Eds.; Springer: Cham, 2019; Vol. 106.

(35) Hayakawa, Y.; Miura, T.; Shizuya, K.; Wakazono, S.; Tokunaga, K.; Kambara, S. Hydrogen Production System Combined with a Catalytic Reactor and a Plasma Membrane Reactor from Ammonia. *Int J Hydrogen Energy* **2019**, *44* (20), 9987–9993. https://doi.org/10.1016/j.ijhydene.2018.12.141.

(36) El-Shafie, M.; Kambara, S.; Hayakawa, Y. Energy and Exergy Analysis of Hydrogen Production from Ammonia Decomposition Systems Using Non-Thermal Plasma. *Int J Hydrogen Energy* **2021**, *46* (57), 29361–29375. https://doi.org/10.1016/j.ijhydene.2020.08.249.

(37) Davies, M.; Cariad Consultants. Corrosion by Ammonia. In *Corrosion: Environments and Industries*; ASM International, 2006; pp 727–735. https://doi.org/10.31399/asm.hb.v13c.a0004185.

(38) Boulos, M. I. Thermal Plasma Processing. *IEEE Transactions on Plasma Science* **1991**, *19* (6), 1078–1089. https://doi.org/10.1109/27.125032.

(39) Snoeckx, R.; Bogaerts, A. Plasma Technology – a Novel Solution for CO_2 Conversion? *Chem Soc Rev* **2017**, *46* (19), 5805–5863. https://doi.org/10.1039/C6CS00066E.

(40) Ju, X.; Liu, L.; Zhang, T.; He, T.; Xu, Y.; Chen, P. Ru Nanoparticles on K Doped γ-Alumina with Abundant Surface Superbasic Sites for Ammonia Decomposition. *Catal Letters* **2024**, *154* (2), 473–486. https://doi.org/10.1007/s10562-023-04317-y.

(41) Nunnally, T.; Gutsol, K.; Rabinovich, A.; Fridman, A.; Gutsol, A.; Kemoun, A. Dissociation of CO_2 in a Low Current Gliding Arc Plasmatron. *J Phys D Appl Phys* **2011**, *44* (27), 274009. https://doi.org/10.1088/0022-3727/44/27/274009.

(42) Vervloessem, E.; Aghaei, M.; Jardali, F.; Hafezkhiabani, N.; Bogaerts, A. Plasma-Based N2Fixation into NOx: Insights from Modeling toward Optimum Yields and Energy Costs

in a Gliding Arc Plasmatron. *ACS Sustain Chem Eng* **2020**, *8* (26), 9711–9720. https://doi.org/10.1021/acssuschemeng.0c01815.

(43) Slaets, J.; Aghaei, M.; Ceulemans, S.; Van Alphen, S.; Bogaerts, A. CO2 and CH4 Conversion in "Real" Gas Mixtures in a Gliding Arc Plasmatron: How Do N2 and O2 Affect the Performance? *Green Chemistry* **2020**, *22* (4), 1366–1377. https://doi.org/10.1039/c9gc03743h.

(44) Stryczewska, H. D. Supply Systems of Non-Thermal Plasma Reactors. Construction Review with Examples of Applications. *Applied Sciences* **2020**, *10* (9), 3242. https://doi.org/10.3390/app10093242.

(45) Boulos, M. I.; Fauchais, P. L.; Pfender, E. *Handbook of Thermal Plasmas*; Springer International Publishing, 2023.

(46) Zhukov, M. F.; Zasypkin, I. M. *Thermal Plasma Torches : Design, Characteristics, Application*; Cambridge International Science Publishing: Cambridge, 2007; Vol. 596.

(47) Girard-Sahun, F.; Biondo, O.; Trenchev, G.; van Rooij, G.; Bogaerts, A. Carbon Bed Post-Plasma to Enhance the CO2 Conversion and Remove O2 from the Product Stream. *Chemical Engineering Journal* **2022**, *442*, 136268. https://doi.org/10.1016/j.cej.2022.136268.

(48) Abello, M. C.; Velasco, A. P.; Gomez, M. F.; Rivarola, J. B. Temperature-Programmed Desorption of NH $_3$ on Na-Y Zeolite. *Langmuir* **1997**, *13* (10), 2596–2599. https://doi.org/10.1021/la960405q.

(49) Liu, C. Y.; Aika, K. Ammonia Adsorption on Ion Exchanged Y-Zeolites as Ammonia Storage Material. *Journal of the Japan Petroleum Institute* **2003**, *46* (5), 301–307. https://doi.org/10.1627/jpi.46.301.

(50) Gillette, J. L.; Kolpa, R. L. *Overview of Interstate Hydrogen Pipeline Systems Environmental Science Division*; Chicago, 2007. https://corridoreis.anl.gov/documents/docs/technical/apt_61012_evs_tm_08_2.pdf (accessed 2024-06-05).

(51) Ariel Corporation. *Application Manual - Heavy Duty Balanced Opposed Reciprocating Compressors*; Mount Vernon, 2023. www.arielcorp.com.

(52) El-Shafie, M.; Kambara, S.; Hayakawa, Y. Energy and Exergy Analysis of Hydrogen Production from Ammonia Decomposition Systems Using Non-Thermal Plasma. *Int J Hydrogen Energy* **2021**, *46* (57), 29361–29375. https://doi.org/10.1016/j.ijhydene.2020.08.249.

(53) Wang, L.-S. *A Treatise of Heat and Energy*; Kulacki, F., Ed.; Mechanical Engineering Series; Springer International Publishing: Cham, 2020; Vol. 301. https://doi.org/10.1007/978-3-030-05746-6.

(54) Mendonça Teixeira, A.; de Oliveira Arinelli, L.; de Medeiros, J. L.; de Queiroz Fernandes Araújo, O. Exergy Analysis of Chemical Processes. In *SpringerBriefs in Petroleum*

Geoscience and Engineering; Springer Nature, 2018; pp 75–82. https://doi.org/10.1007/978-3-319-66074-5_8.

Table of content:

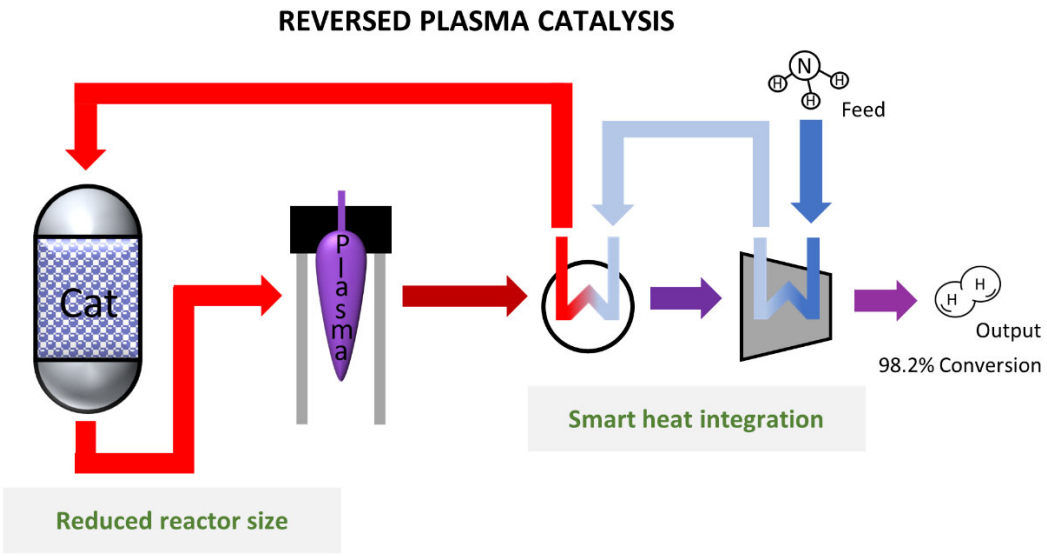

Caption: Schematic overview of reversed plasma catalysis as innovative ammonia decomposition process design with smart heat integration and reduced reactor size as key take-aways.

Supplementary information

Reversed plasma catalysis process design for efficient ammonia decomposition.

Frea Van Steenweghen†[a], Annabel Verschueren†[a], Igor Fedirchyk†[b], Johan Martens*[a], Annemie Bogaerts[b], Lander Hollevoet[a]

[a] *Surface Chemistry and Catalysis: Characterization and Application Team (COK-KAT), KU Leuven, Leuven BE-3001 (Belgium).*
[b] *Research group PLASMANT, Department of Chemistry, University of Antwerp, Wilrijk BE-2610 (Belgium).*
* E-mail: johan.martens@kuleuven.be
†These authors contributed equally

Table of Contents

Table of Figures

Table of Tables

Section 1: Experimental work on thermocatalytic cracking

Catalyst preparation and characterization

The decomposition catalyst is composed of K/Ru/Al_2O_3 with a nominal weight ratio of 10/5/100. γ-Al_2O_3 pellets (Alfa Aesar) were crushed and sieved. The particle fraction of 125-250 µm was calcined for 5 h in air at 550°C. Ru was first loaded on the alumina powder by incipient wetness impregnation with an aqueous solution of $RuCl_3.xH_2O$ (Strem Chemicals Inc, > 99,9%). This powder sample was then dried at room temperature overnight and at 120°C for 5 h, and calcinated in air at 550°C for 5 h (with a heating rate of 1°C.min^{-1}). This powder was defined as 5Ru/Al_2O_3 sample. After cooling, potassium nitrate (KNO_3) (Merck, 99%) was next loaded by incipient wetness impregnation on the 5Ru/Al_2O_3 sample, followed by the same drying and calcination steps. Finally, the sample was again sieved and the 125-250 µm particle fraction was used as catalyst powder to guarantee optimal plug flow through the catalyst bed.

Catalytic decomposition tests

Catalytic NH_3 decomposition tests were performed in a fixed-bed microreactor. A schematic overview of the reactor set-up is given in Figure S1. There were two separate gas flow lines: one for NH_3 and one for H_2, N_2 and He, which came together before entering the reactor. The gasses were supplied by Air Liquide (0-150 mL.min^{-1}). The outlet concentration of all gasses was continuously monitored with a Quadrupole Mass Spectrometer (MS HPR-20 QIC, Hidden Analytical). The outlet flow was sent through an acid trap preventing the uncracked NH_3 to be released in the atmosphere.

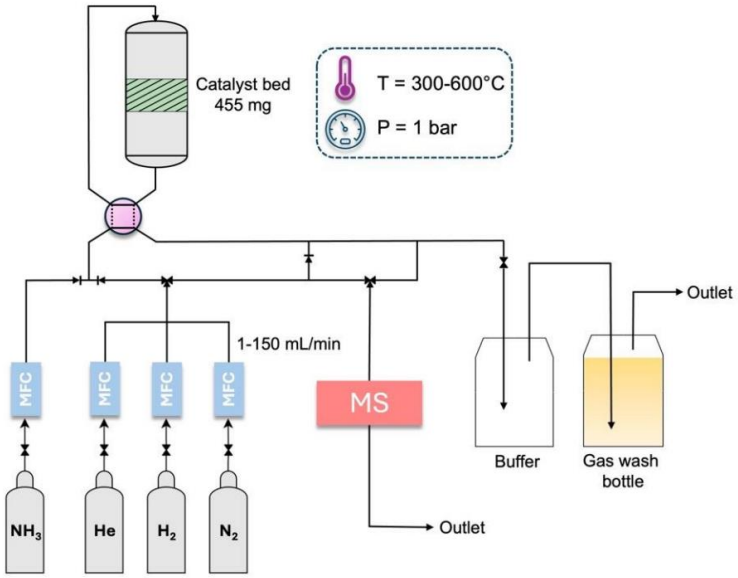

Figure S1: Schematic overview of the ammonia cracking microreactor set-up.

The catalyst pellets (mass = 455 mg, size = 125-250 µm) were fixed in the reactor. A thermocouple was placed inside the catalyst bed. Prior to a cracking experiment, the catalyst was activated in a flowing gas mixture composed of 20 vol% H_2 in N_2 carrier gas at 615°C for 1 h. NH_3 cracking tests were performed at atmospheric pressure at selected temperatures in the range from 615°C to 315°C. The feed gas was pure NH_3 or a mixture produced by the plasma cracking of NH_3 upstream from the catalytic reactor. The weight hour space velocity (WHSV) (h^{-1}) can be calculated with equation S1.

$$WHSV\ (h^{-1}) = \frac{F_{NH_3}^{in}\left(\frac{L}{\min}\right)*60\left(\frac{min}{h}\right)*MW_{NH3}\left(\frac{g}{mol}\right)}{mass_{cat}(g)*V_m\left(\frac{L}{mol}\right)} \quad \text{(S1)}$$

Where $F_{NH_3}^{in}$ is the volumetric flow rate of NH_3 in the feed, MW_{NH3} is the molar weight of NH_3, which is equal to 17 g.mol^{-1}, $mass_{cat}$ is the mass of the catalyst loaded in the reactor, V_m is the molar volume of the feed gas, for which we use 22.4 nL.mol^{-1}. The conversion was calculated from the NH_3 outlet mol fraction (y_{NH3}) (equation S2).

$$NH_3\ conversion = \frac{(1-y_{NH_3})}{1+y_{NH_3}} \quad \text{(S2)}$$

Section 2: Experimental work on plasma cracking

The experimental plasma cracking of NH_3 was conducted using the set-up illustrated in Figure S2. The experimental set-up comprised a gas supply, a plasma reactor connected to a power supply, and an analytics part.

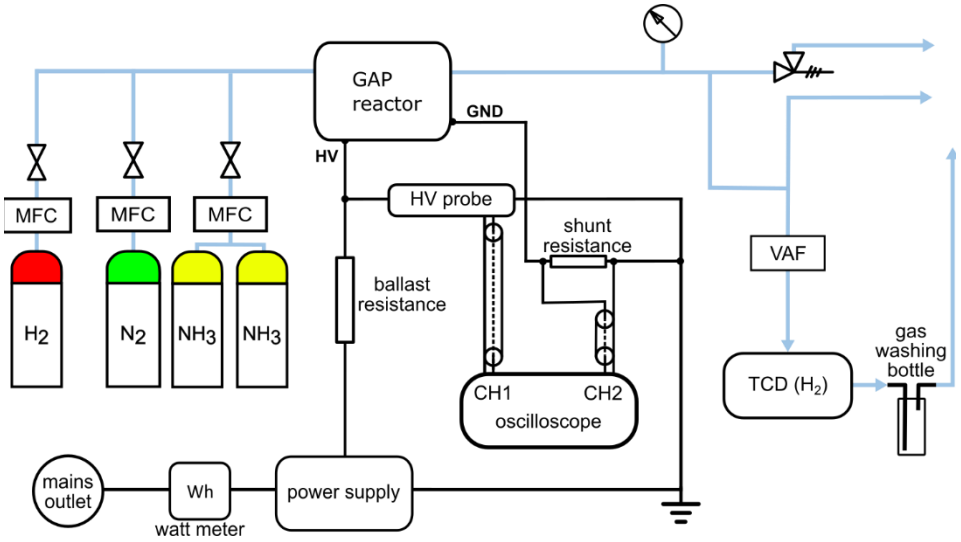

Figure S2: Schematic overview of the plasma reactor set-up for ammonia cracking.

The plasma reactor was based on the Gliding Arc Plasmatron (GAP) design, in which an electric arc is ignited in a vortex flow of gas between two electrodes. It was powered by a current-controlled direct current (DC) linear power supply (Topower Tn-XX02). The power consumed by the plasma reactor (P_{plasma}) was determined from measuring power input into the electric arc using oscillograms of its current and voltage. NH_3 (≈99.96%, Air Liquide), H_2 (≈99.995%, Air Liquide), and N_2 (≈99.999%, Air Liquide) were supplied into the plasma reactor from gas cylinders using Brooks SLA5850 mass flow controllers (MFC). The reactor feed consisted of mixtures of NH_3, H_2 and N_2 corresponding to either pure NH_3 feed or a feed produced by the thermal catalytic cracking of NH_3 upstream from the plasma reactor. The performance of NH_3 cracking via the plasma reactor was evaluated using the following parameters: specific energy input (SEI) per mole of NH_3 in the gas feed, NH_3 conversion (X_{NH_3}), and energy consumption (EC) of decomposing one mole of NH_3. The SEI is calculated using equation S3.

$$SEI\left(\frac{kJ}{mol}\right) = \frac{P_{plasma}\,(W)\cdot 60(\frac{s}{\min})}{1000\,(\frac{W}{kW})\cdot Q^{in}_{NH_3}\left(\frac{Ln}{min}\right)} \cdot V_m\left(\frac{Ln}{mol}\right) \quad \text{(S3)}$$

where $Q^{in}_{NH_3}$ is the mass flow rate of NH_3 in the feed, and V_m is the molar volume of the feed gas, for which we use 22.4 nL.mol^{-1}. X_{NH_3} was calculated from the H_2 concentration in the decomposition products based on the assumption that NH_3 decomposes to a 3:1 mixture of H_2 and N_2 with a statistically insignificant quantity of other byproducts. We must account for gas expansion during NH_3 decomposition because 2 moles of NH_3 decompose into 3 moles of H_2 and 1 mole of N_2. Therefore, X_{NH_3} is equal to (S4):

$$X_{NH_3} = \frac{y^{in}_{NH_3} - y^{out}_{NH_3}}{y^{in}_{NH_3} + y^{out}_{NH_3}} \quad \text{(S4)}$$

where $y^{in}_{NH_3}$ is the fraction of NH_3 in the feed (for the feed containing only NH_3, $y^{in}_{NH_3} = 1$), and $y^{out}_{NH_3}$ is the fraction of NH_3 in the decomposition products. The EC of NH_3 decomposition is calculated using SEI and X_{NH_3} (S5)

$$EC\left(\frac{kJ}{mol}\right) = \frac{SEI(\frac{kJ}{mol})}{X_{NH_3}} \quad \text{(S5)}$$

Section 3: Aspen plus input data

A chemical process model of the *reversed plasma catalysis* process was designed in Aspen Plus V14, as well as of the *plasma catalysis* and *thermocatalysis* process. NRTL was selected as property method. The components NH_3, N_2 and H_2 were inserted. The input of the simulation of the *reversed plasma catalysis* process is given in Table S1. Experimental data were implemented in the simulation. The process schemes of the three processes can be found in Figure S3-S5.

Table S1: Input parameters of the input stream and blocks of the Aspen plus model

	Input parameter	**Value**
Input feed		
	Temperature	-33°C
	Pressure	1 bar
	Flow rate	0.001 $kmol.h^{-1}$
	Mol fraction (NH_3)	1
Heat exchanger (feed – hot product gas)		
	Exchanger specification	Cold stream outlet temperature
	Outlet gas temperature	410°C
	Minimum temperature approach	10°C
Stoichiometric reactor (catalytic)		
	Temperature	410°C
	Pressure drop	0 bar
	Fractional conversion	92.3%
Heater (plasma)		
	Pressure drop	0 bar
	Duty	0.0292 kW
Stoichiometric reactor (plasma)		
	Pressure drop	0 bar
	Duty	0 $cal.s^{-1}$
	Fractional conversion	77.2%
Heater (between hot plasma gas & catalytic reactor)		
	Pressure drop	0 bar
	Duty	-0.0124 kW
Heater (cooling of hot product gas)		
	Temperature	50°C
	Pressure drop	0 bar
Mcomp (compression of product gas)		
	Number of stages	4
	Compressor model	Isentropic using ASME method
	Fix discharge pressure from last stage	50 bar
	Efficiencies: Isentropic	75%[1]

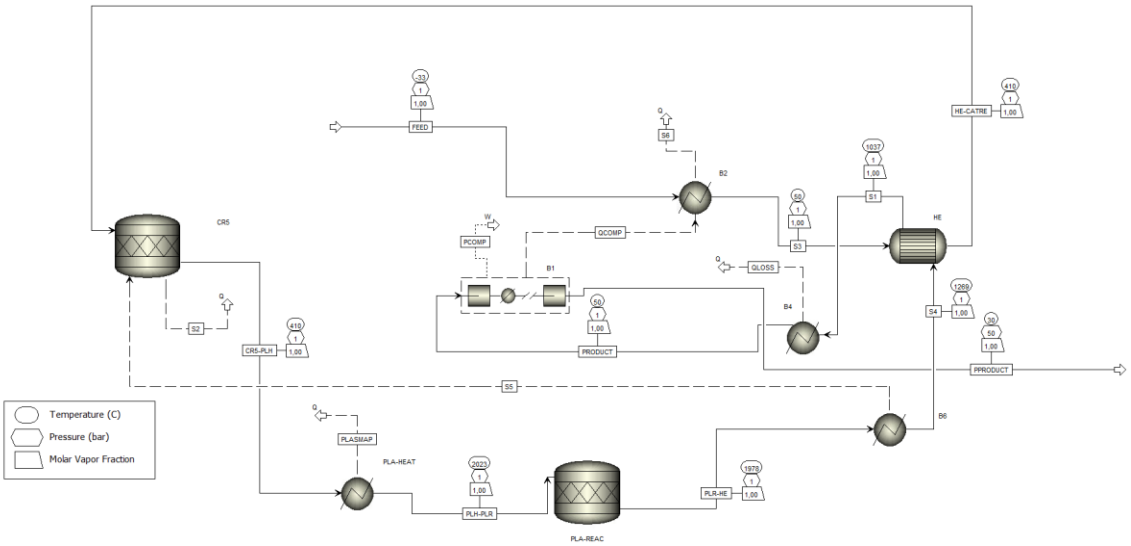

Figure S3: Process scheme of reversed plasma catalysis process with temperature, pressure and molar vapor fraction of all streams, designed in Aspen Plus V14 software.

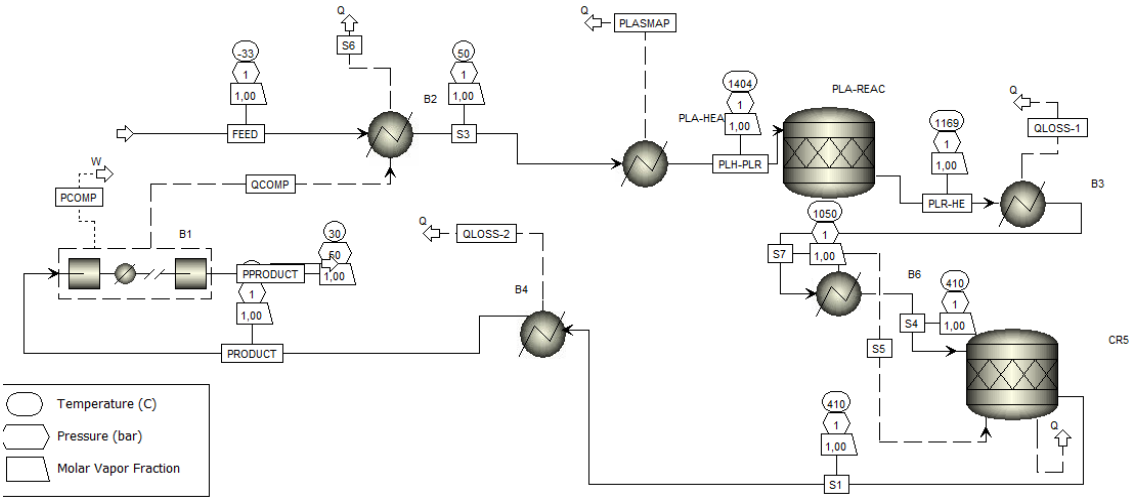

Figure S4: Process scheme of plasma catalysis process with temperature, pressure and molar vapor fraction of all streams, designed in Aspen Plus V14 software.

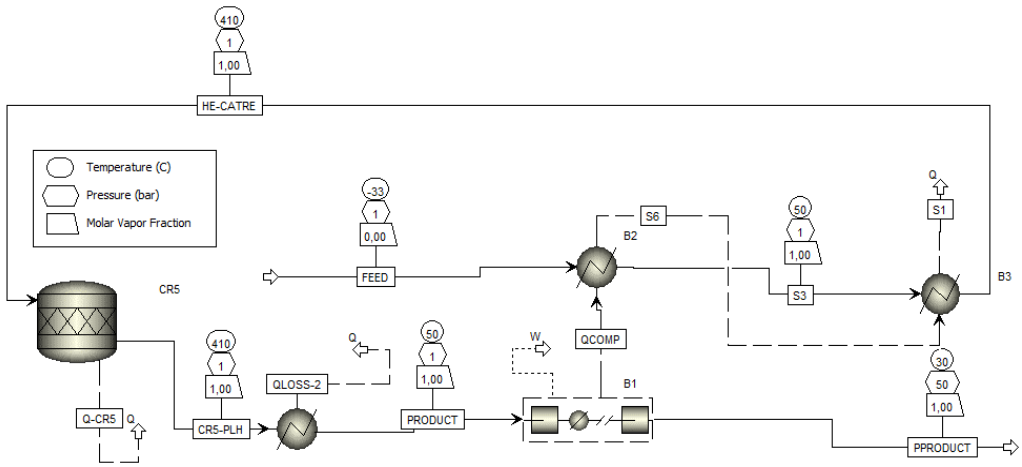

Figure S5: Process scheme of thermocatalysis process with temperature, pressure and molar vapor fraction of all streams, designed in Aspen Plus V14 software.

Section 4: Exergy analysis

A concise exergy analysis was executed to make a correct process comparison between the three experimentally tested and Aspen simulated processes: *thermocatalysis*, *plasma catalysis* and *reversed plasma catalysis*. Exergy can be defined as the available work from an energy source. It takes the quality of the energy into account.

The net exergy consumption is given by the total exergy input minus the useful exergy output.

For the *plasma catalysis* and *reversed plasma catalysis* processes, the total exergy input is the sum of the electrical power of the plasma reactor and of the compressor, together with the chemical exergy of the NH_3 feed. For electricity, the exergy is equal to the applied electrical energy, found in Table S2. For the *thermocatalysis* process, the total exergy input is composed of heating the feed and thermocatalytic reactor, together with the chemical exergy of the NH_3 feed. Heating is assumed to be electrically.

The standard chemical exergy of NH_3 at room temperature (T^0 = 298 K) and atmospheric pressure (P^0 = 1 bar) is 331.5 kJ. mol_{NH3}^{-1} [2]. The chemical exergy of NH_3 at -33°C and atmospheric pressure can be calculated via following formula (S6):

$$Ex_{ch,NH3,-33°C} = Ex^0_{ch,NH3} - T * \Delta S = Ex^0_{ch,NH3} - T * \ln\left(\frac{T}{T^\circ}\right) = 333.3\ kJ.mol^{-1}_{NH3} \quad \text{(S6)}$$

The useful exergy output is the sum of the excess heat generated by the process and the chemical exergy of the product at 5 MPa. This latter can be calculated as a mixture of 75 vol% hydrogen (Ex^0_{H2} = 236.1 kJ.mol_{H2}^{-1} [2]) and 25 vol% nitrogen (Ex^0_{N2} = 0.72 kJ.mol_{N2}^{-1} [2]) (S7):

$$Ex_{ch,mixture} = y_{H2} * (Ex^0_{ch,H2} + R * T * \ln(y_{H2})) + y_{N2} * (Ex^0_{ch,N2} + R * T * \ln(y_{N2})) = 175.7\ kJ.mol^{-1} \quad \text{(S7)}$$

This chemical exergy of the product gas still has to be corrected for the increased pressure (S8):

$$Ex_{ch,product,50bar} = Ex_{ch,mixture} + R * T * \ln\left(\frac{P}{P^\circ}\right) = 185.4\ kJ.mol^{-1}_{product} \quad \text{(S8)}$$

Secondly, the chemical exergy has to be converted to kJ.mol_{NH3}^{-1} (S9):

$$Ex_{ch,product,50bar} = 185.4\ kJ.mol^{-1}_{product} * 2\ \frac{mol_{product}}{mol_{NH3}} * 0.982 = 364.0\ kJ.mol^{-1}_{NH3} \quad \text{(S9)}$$

The excess heat (Q) is converted in exergy via following formula (S10) [3,4]:

$$Ex_{heat} = Q * (1 - \frac{T_h}{T^\circ}) \quad \text{(S10)}$$

Table S2: The exergy input, exergy output and results (net exergy output and exergy efficiency) for both tested configurations: plasma catalysis and reversed plasma catalysis

Process configuration	Plasma catalysis	Reversed plasma catalysis	Thermocatalysis
EXERGY INPUT			
Plasma power (kJ.mol_{NH3}^{-1})	97.6	105.1	
Compressor power (kJ.mol_{NH3}^{-1})	30.9	30.8	29.9
Heating feed & reactor (kJ.mol_{NH3}^{-1})			58.9
Chemical exergy of feed (kJ.mol_{NH3}^{-1})	333.3	333.3	333.3
Total exergy input (kJ.mol_{NH3}^{-1})	461.7	469.2	422.1
USEFUL EXERGY OUTPUT			
Excess heat after plasma reactor (kJ.mol_{NH3}^{-1}) (T_h)	25.4 (1508°C)	36.3 (1978°C)	11.7 (410°C)
Excess heat after heat exchange (kJ.mol_{NH3}^{-1}) (T_h)	11.8 (410°C)	5.5 (263°C)	
Chemical exergy of product (kJ.mol_{NH3}^{-1})	364.0	364.0	364.0
RESULTS			
NET EXERGY CONSUMPTION (kJ.mol_{NH3}^{-1})	60.4	60.5	46.3
EXERGY EFFICIENCY (%)	86.9	87.1	89.0

References:

1 Air Supply UK, A guide to air compressor efficiency: how to calculate and maximise efficiency, https://www.airsupply.co.uk/blogs/a-guide-to-air-compressor-efficiency-how-to-calculate-and-maximise-efficiency/, (accessed 15 November 2024).

2 W. Useng and P. Darul Ridzuan, Bachelor, Universiti Teknologi Petronas, 2011.

3 A. Mendonça Teixeira, L. de Oliveira Arinelli, J. L. de Medeiros and O. de Queiroz Fernandes Araújo, in *SpringerBriefs in Petroleum Geoscience and Engineering*, Springer Nature, 2018, pp. 75–82.

4 L.-S. Wang, *A Treatise of Heat and Energy*, Springer International Publishing, Cham, 2020, vol. 301.